TEM study of structural hardening in a new martensitic steel for aeronautic application

F. Pettinari-Sturmel [a,b,*], B. Kedjar [c], J. Douin [a], C. Gatel [a,b], D. Delagnes [d], A. Coujou [a,b]

[a] CEMES, CNRS, 29 rue Jeanne Marvig, 31055 Toulouse, France
[b] Université de Toulouse, UPS, 29 rue Jeanne Marvig, 31055 Toulouse, France
[c] Institut PPRIME – Université de Poitiers – Département de Physique et Mécanique des Matériaux SP2MI – Téléport 2, 86962 Chasseuneuil-Futuroscope Cedex, France
[d] Université de Toulouse, Mines Albi, ICA (Institut Clément Ader), Campus Jarlard, 81013 Albi cedex 09, France

A B S T R A C T

A new generation of high performance martensitic steel hardened by FeNiAl intermetallic nanoprecipitates has been investigated using conventional and advanced Transmission Electron Microscopy (TEM). Cs-corrected high resolution TEM has been used to provide a fine and accurate microstructural characterization: the shape, size and crystallographic characteristics of the nanoprecipitates have been identified. TEM in situ straining tests have been performed to determine the relevant parameters, which control the deformation. The nanoprecipitates are observed to create anchor lines acting against the propagation of the mobile dislocations and to be crossed by shearing process. In addition, in situ TEM experiments have allowed to measure directly the average distance between these nanoprecipitates along the dislocation lines. This value is of great interest as it is the more accurate data to be used in the calculation of the stress associated with the structural hardening. The strength of the alloy due to these nanoprecipitates has been also determined. It is in good agreement with the value deduced from macroscopic mechanical tests.

Keywords:
Martensitic steels
In situ TEM
Deformation micromechanisms
Dislocation
Precipitation
Structural hardening

1. Introduction

Martensitic steels have been used for decades in a variety of applications (e.g. aeronautics) because of a good combination of yield stress and fracture toughness. The improvement of the mechanical properties has been achieved by a combination of a multiphase precipitation of carbides and of intermetallic nanoprecipitates. It combines the classical beneficial effects of steel hardening with the structural hardening of the maraging steels. In the present aeronautic context, the development and the design of new optimal structural components require a thorough understanding of the mechanical properties in relationship with the interaction between the dislocations and the related microstructure. Thanks to the development of new advanced Transmission Electron Microscopy (TEM) techniques and atom probe analysis, the nanoprecipitation resulting from various thermomechanical treatments has been widely investigated in details in different maraging steels and precisely characterized [1–7]. The distance between the strengthened obstacles is the relevant parameter that controls the propagation of the dislocations and also the deformation mechanisms in a structural hardened alloy. As established by Friedel [8], the value deduced simply from the volume fraction using geometrical calculation is not the relevant one to access to the macroscopic stress. The distance between precipitates along the mobile dislocation line has to be identified. This value can only be obtained using TEM in situ experiment.

This work was thus aimed to contribute to a better understanding of the structural hardening in a new generation of high performance martensitic steel strengthened by intermetallic nanoprecipitates in terms of precipitation characterization and evaluation of its strengthening effect. The originality of this work was to associate for the first time three complementary TEM techniques in the case of such complex alloys. In order to separate the classical steel hardening from the structural hardening, model steels without any carbide have been especially elaborated. The microstructure (sizes, shapes and crystallographic characteristics) of the intermetallic nanoparticles has been precisely investigated using conventional TEM and Cs-corrected High Resolution transmission Electron Microscopy (HREM). The deformation micromechanisms have been investigated using conventional TEM post mortem observations and TEM in situ tensile tests.

2. Experimental

The investigated material is a maraging steel elaborated by Aubert & Duval company with the nominal composition given in Table 1. To produce the expected microstructure, a suitable thermal treatment was applied: an austenitizing treatment for

* Corresponding author at: CEMES CNRS – Université, 29 rue Jeanne Marvig, 31055 Toulouse, France. Tel.: +33 5 62 25 78 73; fax: +33 5 62 25 79 99.
E-mail address: florence.pettinari@cemes.fr (F. Pettinari-Sturmel).

Table 1
Nominal composition of the investigated steel alloy.

	Fe	C	Ni	Cr	Mo	Al	V	Co
wt%	84.8	0.017	11.73	2.38	< 0.01	1.05	< 0.01	< 0.02
at%	84.1	0.078	11.1	2.54	< 0.006	2.16	< 0.011	< 0.019

1 h at 900 °C, followed by a quenching at −80 °C, then a double ageing: at 200 °C for 8 h and then at 500 °C for 10 h. After this treatment the obtained ingot was cut into rectangular rods (1 cm × 1 cm × 20 cm). In addition, some rods were 0.2% plastically deformed at room temperature. In order to identify the effect of the expected intermetallic particles, some samples have been produced without the additional ageing treatment to avoid the intermetallic phase precipitation, and some others without any aluminum to identify the effects of the carbide.

This paper focuses on the TEM results obtained for the thermal heated sample containing Al in order to analyze the interaction between the dislocations and the intermetallic precipitates. The macroscopic tensile tests have been carried out on both samples to point out the structural hardening effect.

The experimental investigations combine three TEM techniques. Conventional post mortem observations (bright field and dark field) on the 0.2% plastically deformed samples and in situ straining experiments were performed using a Jeol 2010 TEM operating at 200 kV equipped with a SIS-CCD camera. The choice of 0.2% plastic strain is usual for post mortem observations of dislocations, as it corresponds to plastically, but not heavily, deformed materials, as during in situ tests. Details on the TEM in situ deformation technique have been specified in previous studies [9,10]. The HREM observations were performed using a FEI-SACTEM (Tecnai F20) operating at 200 kV. This microscope has a field emission gun and is equipped with a spherical aberration corrector (Cs) which allows a point resolution of 0.14 nm in addition of the complete absence of delocalization allowing easier interpretation of contrast.

It is worth emphasizing that TEM observations are very tedious in the particular case of ferritic steels because of difficulties that affect directly the image quality:

- the intrinsic magnetic field due to the ferromagnetic character (85% iron) disrupts the electron beam when the sample is tilted,
- the high internal stresses present in the martensitic alloys cause numerous strong contrasts which make the TEM image difficult to be analyzed.

To minimize the ferromagnetism effect, the volume of the TEM samples is reduced as small as possible, and the surface of a sample should not exceed 1 mm^2. A mechanical thinning has been made to obtain a thickness of 20 μm, followed by an electrolytic etching.

3. Results

3.1. General TEM observations

The general microstructure of the investigated material has been studied using low magnification TEM (Fig. 1). It consists of a well-developed martensite lath structure with relatively straight interfaces between the laths and a high dislocation density within the laths (Fig. 2a). A careful observation of the dislocations reveals extinction contrast along their line (Fig. 2b). These extinctions are

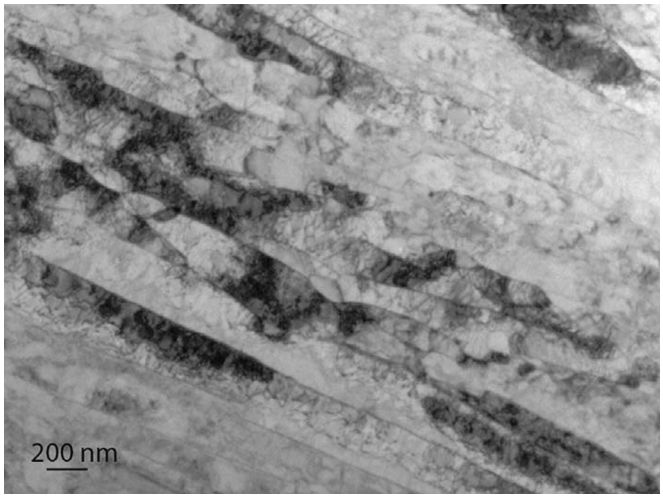

Fig. 1. Conventional TEM micrograph of the martensite lath microstructure.

not oscillating contrasts resulting from dislocation inclinations with the foil but the signature of the interaction between dislocations and nanoparticles. They have been characterized using both conventional TEM and HREM. In structural hardening alloys, the simultaneous observation of precipitates and dislocations is almost impossible because of the compensation of their elastic displacement fields [11]. The dislocation/precipitate interaction changes the contrast of the dislocation line and it can be used to point out the existence of precipitates [12,13]. A schematic representation of the different types of interaction between dislocation and precipitate is illustrated Fig. 3. Different contrasts of the dislocation can be observed either enhanced or blurred out, depending on the applied stress and on the interaction dislocation/precipitate, which can be either attractive or repulsive. Using a qualitative consideration on the total elastic displacement field, the resulting contrast can be predicted:

- in the case of an attractive interaction and for stress-free conditions, thanks to its flexibility, a dislocation would adopt a position as close as possible to the precipitate. It leads to a minimization of the elastic energy i.e. to a minimization of the whole dislocation/ precipitate deformation field. As a consequence, an overall decrease of the dislocation contrast must be observed. In the presence of an applied stress, this situation can be modified. For example, if the stress is sufficient to make the dislocation cross the precipitate, the dislocation contrast disappears and becomes visible again after the shearing process.
- in the case of a repulsive interaction and for stress-free conditions, the dislocation moves away from the precipitate. Its contrast is only slightly modified by the elastic deformation field around the precipitate. Then, if the applied stress makes the dislocation to go closer to the precipitate, the total strain field increases and the dislocation contrast becomes stronger.

These specific variations in the contrast during in situ TEM tests are useful to evidence the location of the precipitates experienced by the dislocations as illustrated in the following.

3.2. Characterization of the nanoprecipitates

In addition to the indexed α-Fe matrix spots, superlattice 100 reflections are observed in $<001>$ zone axis diffraction patterns, whereas they have not been observed in a model alloy without Aluminum. These reflections give a clear evidence of the

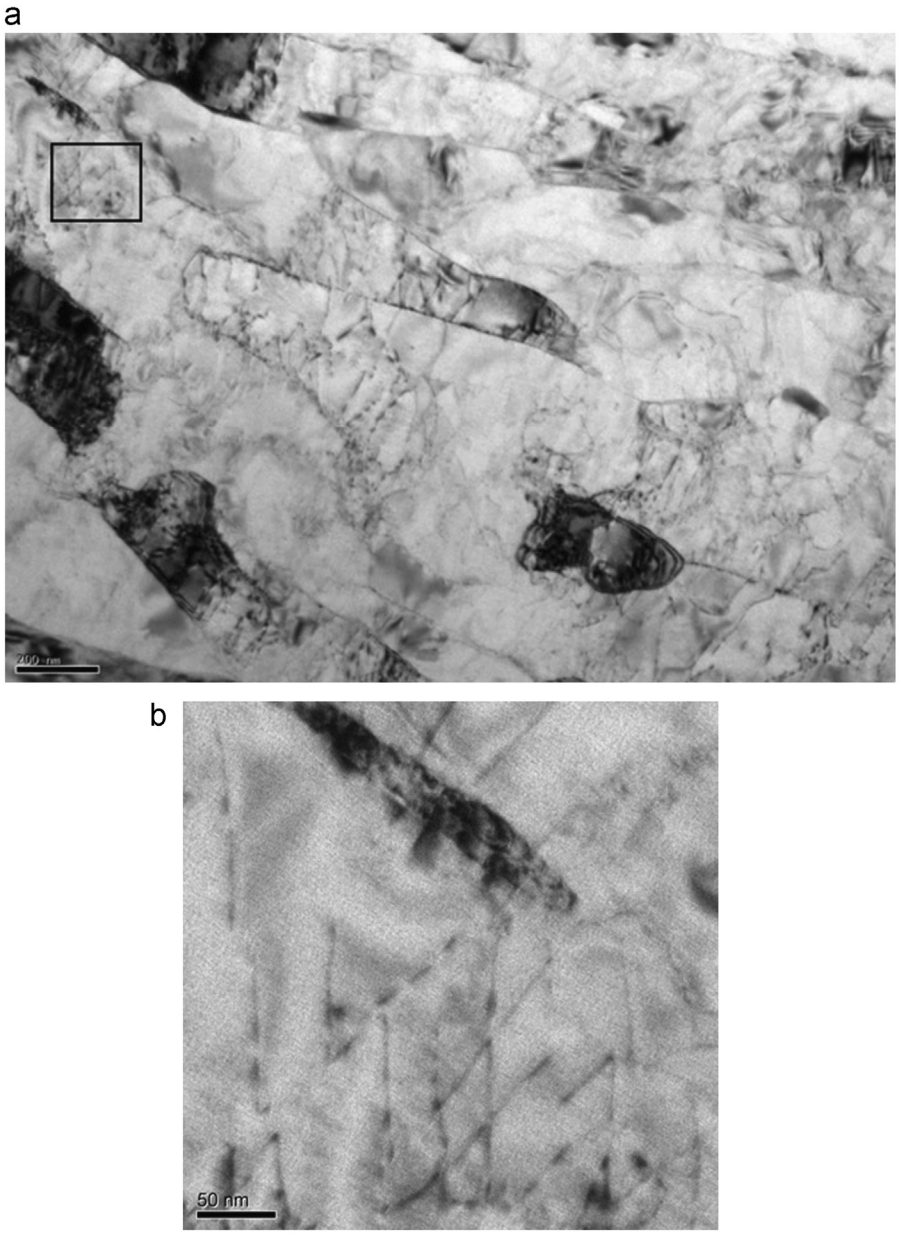

Fig. 2. TEM post mortem observation of dislocations. (a) General overview; (b) Enlargement of the framed area observed in (a). Evidence of changing contrasts along the dislocation lines, which result from the interaction with the nanoprecipitates.

presence of long range order B2 phase. The corresponding dark field (DF) micrograph taken using a 100 reflection from the B2 phase reveals the existence of nanoparticles homogeneously distributed in the martensitic matrix (Fig. 4). Their size ranges around 2–3 nm but can only be roughly estimated using such micrograph.

In order to get a precise microstructural analysis of these precipitates, additional HREM observations were performed. The micrograph illustrated Fig. 5a is to a Cs corrected HREM image taken along a $<001>$ zone axis of the matrix. This HREM image shows a large monocrystalline area suggesting a good crystalline quality of the alloy. A nanoparticle is located at the center of the image (in the area 2). The corresponding Fourier Transform (FT) allows to point out again 100 superstructure spots in addition to the expected cubic centered α-Fe matrix spots. The lattice parameter has been measured from HREM experiment. It is about ~0.29 nm. The orientation relationship is found to be $[1\,0\,0]_{B2}//[1\,0\,0]_{\alpha}$ in agreement with the classical one proposed by Erlach et al. [5] (for sake of simplicity, we have considered the α-Fe matrix to be cubic instead of tetragonal; the theoretical lattice parameters calculated using the chemical composition as proposed by Cheng et al. [14] are: $a=0.2866$ nm and $c=0.2868$ nm). The precipitate is thus observed to be coherent with the matrix.

As the precipitates are embedded in the matrix, the exact position of the interface between precipitate and matrix is not so easy to be determined. The atomic column contrasts have been enhanced using image filtering. Then, the corresponding intensity profiles have been plotted to identify more easily the position of the interface. Assuming a spherical shape, the radius of the precipitates has been measured with an accuracy of few atomic planes. It is 2.4 ± 0.5 nm as deduced from statistical analysis.

3.3. TEM in situ deformation: dislocation – precipitate interaction

3.3.1. Experimental observations

A high dislocation density has always been observed in the sample before the tensile test. It suggests that the elaboration

process induces a large work hardening. This high dislocation density makes the investigation of the elementary deformation micromechanisms particularly difficult. We have then focused on the less deformed areas where the propagation of individual dislocations is easier and can be analyzed.

An example of interaction between dislocations and precipitates observed during an in situ straining experiment is illustrated Fig. 6. Using the diffraction vector $g = \overline{1}\,\overline{1}2$, the dislocations and most of the precipitates are observed. A lower density of dislocations is observed in area B in comparison with the area A. The under stress mobile dislocations observed in this area B have a $a/2[\overline{1}11]$ Burgers vector. During their motion, the dislocations are preferentially aligned along their screw orientation. They are pinned by the precipitates and are observed to shear them. Some open glissile loops are observed (Fig. 6 see 1–3). These loops are probably formed by cross slip of the screw dislocations as reported by several authors [13,15,16]. There are also some small Orowan loops (Fig. 6 see 5) resulting from precipitate by-passing. Although some evidences of Orowan by-passing have been observed, the shearing mechanism is the prevalent one.

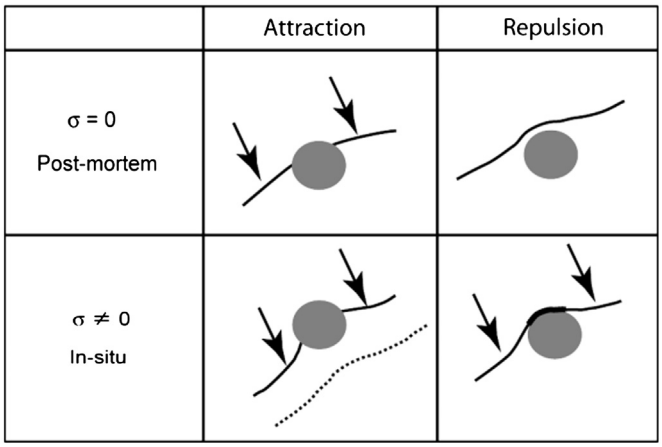

Fig. 3. Schematic representation of the resulting contrast from the interaction between dislocation and precipitate. Different situations are proposed: attractive and repulsive interactions, for stress-free or under stress dislocation.

As already mentioned, the presence of precipitates can be evidenced by a minimization or an enhancement of the local dislocation contrast, depending on the stress and on the nature of the precipitate/dislocation interaction. During the in situ sequence illustrated Fig. 6**,** the contrast is observed to become stronger when dislocations approach the precipitates (as indicated by the white arrows). Thus it corresponds to a case of a repulsive interaction between precipitates and dislocations.

Another in situ straining experiment is shown Fig. 7. In the initial state the dislocation is locked in the position 1 (Fig. 7a). The contrast of some nanoprecipitates located along the dislocation line is enhanced due to the interaction with the pinned dislocation (see for example in *i, j, k* and *m* Fig. 7a). Then the dislocation jumps and stops again along others anchor points at the position 2 (Fig. 7b). Here again, the interaction between the precipitates and the nano-obstacles allows to enhance their contrast (noted *n, o,* and *p*). Some precipitates (noted *q* and *r*) are evidenced now because of their interaction with the dislocation.

These TEM in situ tensile tests appear then to be the appropriate tool and the unique one to determine the distance between the precipitates along a dislocation line in its motion plane. This parameter is a key one for the structural hardening understanding as it allows a quantitative location of the efficient obstacles encountered by a dislocation in its glide plane. The corresponding results are given in the following.

3.3.2. *Distance between precipitates along an anchor line*

The average distance between precipitates along an anchor line has been deduced from TEM in situ sequences. In order to determine the real distances from the projected ones, some simple geometric corrections have to be used [12]. For evident convenient reasons, the experimental measurements have been performed only in the case of contrast enhancement as illustrated previously. All the experimental data obtained are summarized in the histogram illustrated Fig. 8. It can be deduced that the average distance between precipitates is 53 ± 2 nm.

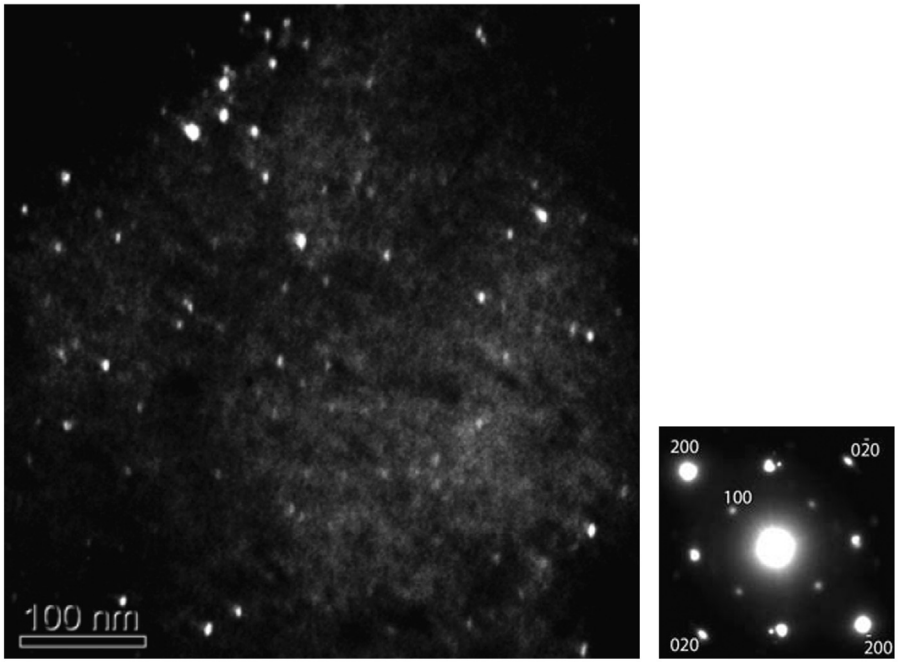

Fig. 4. Dark field TEM micrograph using a superlattice **100** reflection evidenced in the $< 001 >$ zone axis diffraction pattern.

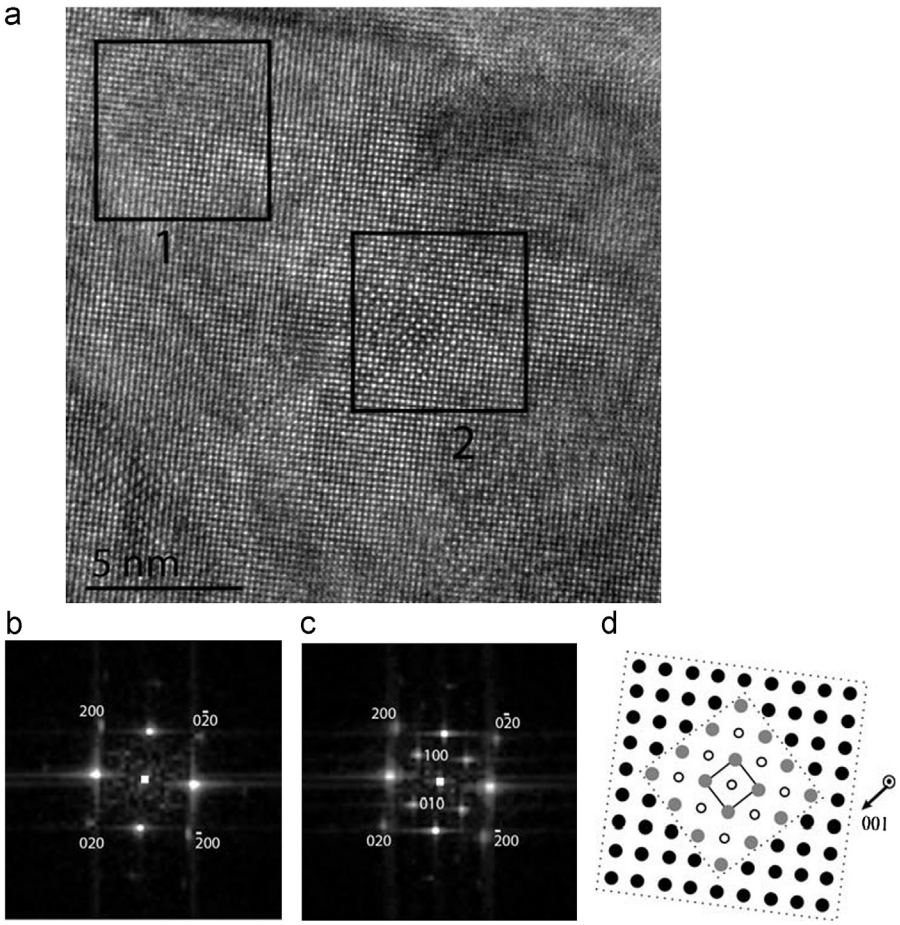

Fig. 5. (a) HREM micrograph ; (b) and (c) Fourier Transforms corresponding respectively to the area 1 and 2. The additional **100** reflections observed in (c) correspond to the nanoparticle imaged in area 2 and reveal a B2 ordered structure. (d) Schematic representation of an intermetallic ordered nanoparticle (in the center) imbedded in the Fe-matrix, observed along the [001] direction.

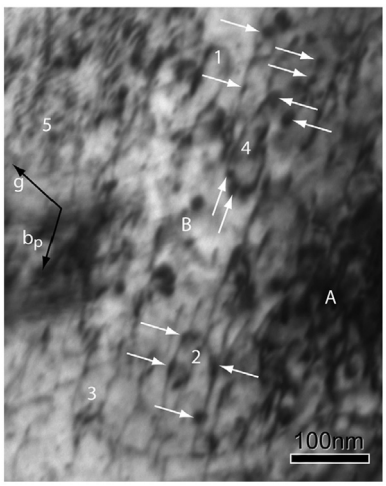

Fig. 6. TEM in situ observation of mobile dislocations at room temperature. The arrows indicate the presence of precipitates along the dislocation line.

4. Discussion

In the following, the nature of the B2 ordered particles is first discussed and compared with the literature. Then, using the experimental data, a quantitative analysis of the structural hardening is proposed and compared with macroscopic results.

4.1. About the nature of the ordered precipitates

The experimental results obtained from dark field TEM and HREM can be interpreted as an evidence of B2-NiAl intermetallic phases as reported in the literature for similar steels. For example, Taillard and Pineau [2] have studied the precipitation in FeNiCrAl alloys after annealing at 650 °C for 6.5 h and have found a precipitation of B2 ordered NiAl particles coherent with the matrix. Their size ranges around 25 nm. Similar B2-NiAl particles have been also identified by other authors [5,17,18]. One may also suggest the existence of B2-FeAl intermetallic precipitates. Both intermetallics have an ordered B2 structure and a lattice parameter in agreement with ours (0.2865 nm for B2-FeAl and 0.2887 nm for B2-NiAl). Using experiment and simulation [7,19,20], it has been well established that Fe atoms may occupy the Al or Ni sites in the ternary FeNiAl where there is a strong tendency to maximize the Ni–Al and Fe–Al interactions and B2-FeNiAl particles with similar size as ours have been reported. To conclude, we may describe the intermetallic precipitates present in the alloy under study as B2-FeNiAl nanoparticles.

4.2. Quantitative analysis of the structural hardening

The intermetallic nanoparticles causes an increase of the macroscopic strength: the macroscopic yield stress obtained for the investigated alloy containing intermetallic precipitates is 1170 MPa, whereas it is 850 MPa in the case of the quenched alloy

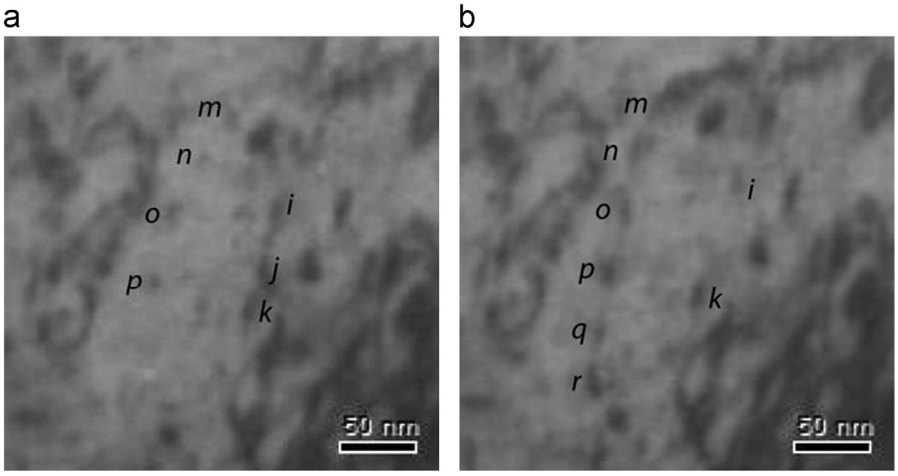

Fig. 7. TEM in situ sequence illustrating two positions of a dislocation line along anchor line created by nanoprecipitates. (a) The dislocation is observed in a first position being anchored on the precipitates noted at their right side *i, j, k*; (b) the dislocation is observed to be pinned by all the precipitates noted at their left side from *m* to *r*. The interaction with all of them induces a contrast enhancement. The precipitates *q* and *r* were not in contrast in the micrograph *a* because of the absence of the dislocation.

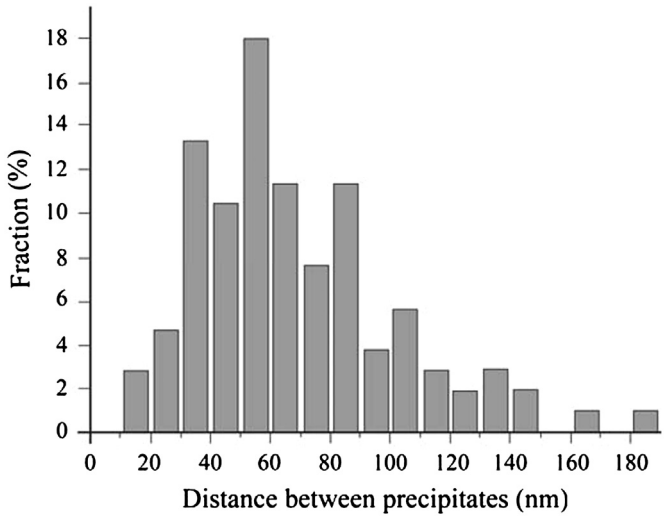

Fig. 8. Experimental distances between precipitates along a dislocation line.

i.e. without any precipitate. An attempt has been made to link the experimental data obtained at the microscopic scale to this macroscopic strengthening increase $\Delta\sigma = 1170–850 = 320$ MPa. At a first approximation, the relationship proposed by Friedel for a dislocation curved between two obstacles (forest dislocations) has been used [8] (the details for the calculation are reported in the appendix):

$$\Delta\tau = T/Rb = (2T\ell_1^2)/(\ell_2^3\, b)$$

where T is the line tension evaluated in the framework of isotropic elasticity i.e. $T \approx \mu.b^2$ with μ (80 GPa) the shear modulus, R the dislocation curvature radius, b (0.25 nm) the Burgers vector of the dislocation, ℓ_1 the "geometrical distance" between precipitates i.e. deduced from the precipitate volume fraction f_v [21] and ℓ_2 the distance between the efficient precipitates, which act as obstacles i.e. the distance between the anchored points along the dislocation line deduced from TEM in situ test. Using $\ell_1 \approx 13$ nm and $\ell_2 \approx 53 \pm 2$ nm (as measured), a stress of about 50 ± 2 MPa has been found (see Appendix for more details). This is highly lower than the macroscopic value. In fact, this approach does not take into account the nature of the obstacle. As they are ordered particles, the interaction between the dislocations and these precipitates has to be considered precisely.

4.3. Quantitative analysis of the deformation micromechanism associated with the structural hardening

When an under stress mobile dislocation is stopped by precipitates, two mechanisms may occur: the Orowan by-passing or the shearing process. The occurrence or the prevalence of one of these mechanisms can be deduced unambiguously using TEM in situ experiment. Here, many evidence of shearing mechanisms have been observed whereas Orowan by-passing is rare. In addition to these qualitative observations, the main quantitative parameters involved in both mechanisms, which are the size of precipitates, the distance between neighboring precipitates, the nature of the dislocation, the cross-slip and climb possibility, and of course the stress level, can also be deduced from in situ experiments.

The τ_{OR} stress associated with the Orowan mechanism for a dislocation with a line tension T, a Burgers vector b propagating between precipitates separated by the distance ℓ_2 can be calculated using:

$$\tau_{OR} = 2T/b\ell_2$$

Using the experimental data $\ell_2 \approx 53 \pm 2$ nm, we have found $\tau_{OR} \approx 706 \pm 30$ MPa.

As the precipitates are B2 ordered phases, their shearing by a perfect $<1\,1\,1>$ matrix dislocation requires the creation of a planar defect in the precipitate, the so-called Anti-Phase Boundary (APB) with the associated energy γ_{APB}. The knowledge of the necessary stress associated with these mechanisms is of particular interest as it reflects the obstacle strengthening. The τ_{APB} stress required for ordered precipitates to be sheared has been calculated by Hüther and Reppich [22]. In their calculation, the influence of the line tension, which assists the applied stress is taken into account. The necessary stress to propagate the dislocation in an ordered precipitate is then given by:

$$\tau_{APB} = \gamma_{APB} D/b(\ell_2 + D)$$

where D is the diameter of the precipitate ($D = 4.8$ nm).

Only few values of γ_{APB} are available in the literature for FeNiAl alloys. For example in 50Fe–10Ni–40Al alloy, Savage et al. [23] have found $\gamma_{APB} = 500$ mJ/m^2 for an APB in the (110) plane from the dislocation dissociation distance measurements. These authors have also reported that addition of Ni contributes to the increase of γ_{APB} in FeNiAl alloys. Elsewhere, using atomic calculation different values have been found: 990 mJ/m^2 for NiAl in the (112) plane and 810 mJ/m^2 in the (110) plane [24]. If we consider

the minimum value for γ_{APB} i.e. $\gamma_{APB}=500$ mJ/m^2, we find that the minimum necessary stress to shear the precipitates is $\tau_{APB}=170$ MPa, which is much lower than the Orowan stress and explains the prevalence of the shearing process.

The aim of our approach was to propose a quantitative approach of the structural hardening in a complex steel using experimental analysis. The originality of this tedious work can be summarized as follows:

- the shearing mechanism has been observed to be the prevalent mechanism although Orowan by-passing has been mainly reported in similar steels [2]. This is in agreement with the calculated Orowan stress, which is much higher than the shearing stress in our case. Notice that the Orowan stress has been determined in other papers [25,26]; it ranges around 100 MPa, but the situation is completely different: it concerns carbides with a larger spacing (between 280 and 400 nm) and with larger size (between 20 nm and 50 nm for the diameter).
- the calculated stresses associated with the shearing process gives a quantitative result on the strength due to the nanoprecipitates. It gives thus an estimation of the structural hardening effect. It has to be compared with the macroscopic additional stress determined by the difference in the yield stresses obtained for the steel with and without nanoprecipitates, which is 320 MPa. There is a wide range of γ_{APB} values in the literature (from 500 mJ/m^2 to 900 mJ/m^2). In single-phased FeNiAl alloys, γ_{APB} increases with Ni content (500 mJ/m^2 for 10% Ni [23]). In our material, the global stoichiometry is around 10%Ni, thus the actual Ni stoichiometry in the FeNiAl nanoprecipitates is much larger than 10%. It is then believed that γ_{APB} tends to the highest values (up to 900 mJ/m^2). The calculated stress then approaches 300 MPa in agreement with the macroscopic tests. It corresponds to 20% of the elastic limit.
- Finally, the main result is that the knowledge of the distance between the precipitates along the dislocation line is of great interest for a fine analysis of the structural hardening. Indeed, in the case of curved dislocations, the "geometrical" distance between precipitates deduced from the volume fraction can highly differs from the relevant one and may lead to uncorrected result. Here a value of 13 nm as deduced from a simple microstructural analysis without taking into account the interaction with the dislocations would give a shear stress between 540 MPa and 975 MPa. In addition, the fitting of the experimental stress to the calculated one is a possible way to access to the antiphase boundary energy, which is quite impossible to be obtained in the investigated alloy.

5. Conclusion

This work was aimed to correlate as fine as possible the microstructure and the deformation micromechanisms to the macroscopic behavior in a martensitic steel hardened by intermetallic nanoprecipitates, combining three different TEM techniques for the first time in such an alloy. The conventional TEM and particularly the HREM has allowed to obtain a precise description of the nanoprecipitates in agreement with the literature: they are fairly spherical with a radius close to 2.4 nm, they are coherent with respect to the matrix and of B2 ordered type. For the first time, the interactions between intermetallic nanoparticles and under stress mobile dislocations have been observed and analyzed quantitatively in such steel using TEM in situ tests. The shearing of these FeNiAl ordered nanoprecipitates has been clearly evidenced as the controlling deformation mechanism. The average distance between precipitates along a mobile dislocation line has been determined. Then, the necessary stress to shear the precipitates has been calculated: it ranges from 170 MPa to 310 MPa depending on the γ_{APB} energy. It represents 20% of the elastic limit measured in the investigated steel and is always lower than the necessary stress for an Orowan by-passing. It corresponds to the additional macroscopic strength caused by the structural hardening and is in agreement with macroscopic tensile tests.

Acknowledgments

The French National Agency (ANR) is gratefully acknowledged for financial support (ANR-05-RNMP-08).

Appendix

Assuming a surface density N_s of spherical precipitates with radius r, arranged in a square lattice, the spacing ℓ_1 between two neighbor precipitates can be written as [8,21]:

$$\ell_1 = 1/N_s^{0.5} \tag{A.1}$$

with $f_v=N_s\,\pi r_s^2$ and $r_s=(2/3)^{0,5}\,r$, with r_s being the mean radius of precipitates in the slip plane, then:

$$\ell_1 = \sqrt{2\pi/3f_v}\;\; r \tag{A.2}$$

Using the experimental value for $r=2.4$ nm and the precipitate volume fraction $f_v=7.2\%$ deduced from Small Angle Neutron Scattering [27] it has been found: $\ell_1=13$ nm.

In fact, the distance between precipitates along a dislocation line is not equal to ℓ_1: it should be ℓ_1 if the dislocation were perfectly flexible. This is not the general case. The dislocation line tension T, the dislocation curvature radius, the additional stress $\Delta\sigma$ due to the structural hardening and the relevant distance ℓ_2 between precipitates along the dislocation line (i.e. the distance between the precipitates, which anchor the dislocation) are linked by the following equations proposed by Friedel (in the case of wavy obstacles) [8]:

$$\Delta\tau = T/Rb = (2\,T\ell_1^2)/(\ell_2^3\,b) \tag{A.3}$$

Then using, the line tension evaluated for a screw dislocation (as it corresponds to the experimental cases):

$$T = \frac{\mu b^2}{4\pi}\left(\frac{1+\nu}{1-\nu}\right)\ln\frac{L}{r_0} \tag{A.4}$$

with L ($\approx$200 nm) being the grain size, r_0 being equal to the Burgers vector b (0,25 nm), μ the shear modulus (80 GPa) and ν(1/3)1/3 the Poisson ratio, we find $T=0.99\ \mu b^2 \sim \mu b^2$.

References

[1] K. Stiller, F. Danoix, A. Bostel, Appl.Surf. Sci. 94-95 (1996) 326–333.
[2] R. Taillard, A. Pineau, Mater. Sci. Eng. 54 (1982) 209–219.
[3] C. Stallybrass, G. Sauthoff, Mater. Sci. Eng. A 387 (2004) 985–990.
[4] E. Courtois, T. Epicier, C. Scott, Micron 37 (2006) 492–502.
[5] S.D. Erlach, H. Leitner, M. Bischof, H. Clemens, F. Danoix, D. Lemarchand, I. Siller, Mater. Sci. Eng. A 29 (2006) 96–106.
[6] P. Michaud, D. Delagnes, P. Lamesle, M.H. Mathon, C. Levaillant, Acta Mater. 55 (2007) 4877–4889.
[7] S. Höring, N. Wanderka, J. Banhart, Ultram 109 (2009) 574–579.
[8] J. Friedel, Dislocations, Oxford Pergamon Press223–225.
[9] A. Couret, J. Crestou, S. Farenc, G. Molénat, N. Clément, A. Coujou, D. Caillard, Microsc. Microanal. Microstruct. 4 (1993) 153–170.
[10] F. Pettinari, A. Couret, D. Caillard, G. Molénat, N. Clément, A. Coujou., J. Microsc. 203 (2001) 47–56.
[11] R.M. Allen, J.B. Vandersande, Metall. Trans. A 9 (291) (1978) 1251–1258.
[12] F. Delmas, Ph.D. Thesis, Toulouse Université Paul Sabatier 2002.
[13] F. Delmas, M. Vivas, P. Lours, MJ Casanove, A. Couret, A. Coujou, Mater. Sci. Eng. A 340 (2003) 286–291.

[14] L. Cheng, N.M. Van Der Pers, A. Böttger, TH De Keijser, EJ. Mittemeijer, Metall. Trans. 22A (1991) 1957–1967.
[15] A.J.E. Foreman, P.B. Hirsch, F.J. Humphrey, J. Res. Natl. Bur. Stand. sect. A-Phys. Chem. A73 (1969) 532–540.
[16] E.J. Furubayashi, J. Phys. Soc. Jpn. 27 (1969) 130–146.
[17] Z. Guo, W. Sha, D. Vaumousse, Acta Mater. 51 (2003) 101–106.
[18] D.H. Ping, M. Ohnuma, Y. Hirakawa, Y. Kadoya, K. Hono, Mater. Sci. Eng. A 394 (2005) 285–295.
[19] G.H.. Bozzolo, J. Khalil, RD. Noebe, Comput. Mater. Sci. 24 (2002) 457–480.
[20] R. Banerjee, S Amancherla, S. Banerjee, H.L. Fraser, Acta Mater. 50 (2002) 633–641.
[21] V. Gerold in: Nabarro FRN (Ed.), Dislocations in solids, vol. 4, 1979.
[22] W. Hüther, R. Reppich, Z. Metallk. 69 (1978) 628–634.
[23] M.F. Savage, R. Srinivasan, M.S. Daw, T. Lograsso, M.J. Mills, Mater. Sci. Eng. A 258 (1998) 20–25.
[24] C.L. Fu, M.H. Yoo, Acta Metall. 40 (1992) 703–711.
[25] K. Maruyama, K. Sawada, J. Koike, ISIJ Int. 41 (2001) 641–653.
[26] S. Maropoulos, J.D.H. Paul, N. Ridley, Mater. Sci. Tech. 9 (1993) 1014.
[27] D. Delagnes, F. Pettinari-Sturmel, M.H. Mathon, R. Danoix, F. Danoix, C. Bellot, P. Lamesle, A. Grellier, Acta Mater. (2012) 5877–5888.